## Deliverable Flexible Ramping Products Considering Spatiotemporal Correlation of Wind Generation and Demand Uncertainties

Xin Fang, Senior Member, IEEE; Kwami Senam Sedzro, Senior Member, IEEE; Haoyu Yuan, Member, IEEE; Hongxing Ye, Senior Member, IEEE; Bri-Mathias Hodge, Senior Member, IEEE

Abstract— Flexible ramping products (FRPs) have been implemented by several independent system operators (ISOs) to procure adequate flexible resources. Currently, system operators estimate the system level ramping requirements ignoring the spatiotemporal correlations among various uncertainty sources. This leads to overestimates/underestimates of ramping requirements. In addition, the explicit FRPs model considers only the generation ramping limitation. Other security constraints, such as the transmission limits, are not considered, which leads to deliverability issues of FRPs. To deal with these shortcomings of current FRPs models, this paper proposes a deliverable FRPs based on a distributionally-robust chance constrained multiinterval optimal power flow (DRCC-MIOPF) considering the spatiotemporal correlation of wind power and demand uncertainties endogenously. Furthermore, an asymmetrical affine policy (AAP) is proposed to leverage generation flexibility and mitigate the uncertainty in different directions. The pricing mechanism of the FRPs is proposed using a novel uncertaintycontained locational marginal price (U\_LMP) which is derived from the proposed AAP-DRCC-MIOPF model. New components representing the price of FRPs are added into the traditional LMP formulation. Finally, the PJM 5-bus, IEEE 39-bus and IEEE 118bus systems case studies validate the proposed FRPS approach. The payment of uncertain demand and wind power on FRPs are analyzed.

Index Terms— Flexible ramping products (FRPs), Spatiotemporal correlation, electricity market, locational marginal price (LMP).

#### NOMENCLATURE

$c_{i,t}$	Generator <i>i</i> bid price (\$/MWh) at time <i>t</i> ,
$G_{i,t}$	Power output of generator $i$ (MW) at time $t$ ,
$G_i^{max}/G_i^{min}$	Generator <i>i</i> upper/lower limits (MW),
$D_{i,t}$	Demand level (MW) at bus $i$ at time $t$ ,
$P_{i,t}$	Wind power (MW) at bus $i$ at time $t$ ,
$GSF_{l,i}$	Generation shift factor of bus <i>i</i> to line <i>l</i> ,
$LU_{l}$	Line limit of line <i>l</i> ,
$G_{exp,i,t}$	Generation output of generator at bus $i$ (MW)
• • •	at time t under forecasted wind and demand,
$P_{exp,i,t}$	Forecast wind power (MW) at bus $i$ at time $t$ ,
$D_{exp,i,t}$	Forecast demand (MW) at bus $i$ at time $t$ ,
$eta_{i,t}$	Generation balancing factor for the system
	imbalance at bus $i$ at time $t$ ,
$eta_{U,i,t}$	Generation balancing factor for the up
	reserve at bus <i>i</i> at time <i>t</i> ,

This work was coauthored by Alliance for Sustainable Energy, LLC, the Manager and Operator of the National Renewable Energy Laboratory for the U.S. Department of Energy (DOE) under Contract No. DE-AC36-08GO28308. Funding provided by U.S. Department of Energy Office of Energy Efficiency and Renewable Energy Wind Energy Technologies Office. H. Ye's work is supported by U.S. National Science Foundation under project no. EECS-1711217.

$eta_{D,i,t}$	Generation balancing factor for the down
	reserve at bus $i$ at time $t$ ,
$\Delta G_{i,t}$	Generation corrective power response to
.,-	mitigate the system uncertainty at time $t$ ,
$\Delta P_{i,t}$	Wind power output uncertainty at time $t$ ,
$\Delta D_{i,t}$	Demand uncertainty at time t,
$PF_{l,t}$	Active power flow on $l^{th}$ line at time $t$ ,
$\xi_{d,j,t}$	Percentage of standard deviation to expected
-	value of demand at time <i>t</i> ,
$\xi_{w,j,t}$	Percentage of standard deviation to expected
-	value of wind power at time <i>t</i> ,
$f_{exp}$	Generation cost corresponding to the
	forecasted wind and demand,
Ξ	Sparse covariance matrix of wind power and
	demand forecast errors,
$\sigma_{i,t}$	Standard deviation of wind power plant
	(WPP) $i$ -th power forecast error at time $t$ ,
$\sigma_{PF,l,t}$	Standard deviation of the power flow on the
	<i>l</i> -th transmission at time <i>t</i> ,
$\sigma_{g,i,t}$	Standard deviation of the <i>i</i> -th generation
	unit's power output at time t,
$R_i^U/R_i^D$	Ramp-up/-down limits (MW/minutes) of the
	<i>i</i> -th generation unit,
$\Delta t$	Length of the time interval (minutes) in the
	studied multi-interval model,
$Ramp_{i,t}$	Generation $i$ 's power ramp at time $t$ ,
$r_{g,i,t}$	Standard deviation of the generation i's ramp

The other variables will be explained in the text.

at time t.

## I. INTRODUCTION

LEXIBLE ramping products (FRPs) have been implemented by several independent system operators (ISOs) such as California Independent System Operator (CAISO) and Midcontinent Independent System Operator (MISO) to procure adequate flexible ramping resources for mitigating system imbalances because of renewable power and demand forecast errors in their real time operation [1], [2]. In these designs, specifically in the real-time markets, the flexible ramping capacity is reserved by adding additional ramping requirements in the original real-time economic dispatch (RTED) models [3], such that the FRPs are co-optimized with energy and other ancillary services. In this type of models, the

Xin Fang, Kwami Senam Sedzro, Haoyu Yuan, and Bri-Mathias Hodge are with the National Renewable Energy Laboratory, Golden, CO, 80401, USA.

Bri-Mathias Hodge is also with the University of Colorado Boulder and the Renewable and Sustainable Energy Institute.

Hongxing Ye is with the Cleveland State University, Cleveland, OH 44115 USA.

ramping requirements are usually evaluated based on the system net-load variation [4].

Current FRPs models consider the generation ramping limitation in the RTED [5]. However, the impacts of the flexible ramping capacity on other system security constraints such as the transmission limits are not considered. This might lead to deliverability issues of the FRPs in real time operation. To deal with these issues, Ref. [6] proposed an approach to address the reserve capacity deliverability on a zonal basis considering the system's discrete contingencies. The bus-level delivery of the ramping capabilities has not been addressed in this study. Ref. [7] proposed the deliverable ramping products considering transmission constraints and the deliverability of ramping products through a robust optimization model. In this model, the uncertainty of demand and wind power were represented using the interval uncertainty sets which did not take the spatiotemporal correlations of demand and wind power uncertainties into consideration. Similarly, Ref. [8] proposed an uncertainty marginal price based on robust optimization in the unit commitment problem ignoring the spatiotemporal correlation. Ref. [9] demonstrated that considering the spatiotemporal correlation of the renewable power outputs and the system electricity demand could bring reliability and economic benefits in system ramping requirements evaluation.

However, it is still challenging to consider the spatiotemporal correlations of uncertain demand and wind power, which might lead to overestimating/underestimating the system ramping requirements. These misestimates of ramping requirements will affect not only the generation schedules and system operating costs, but also result in system security risks. In addition, currently demand pays the total cost of ancillary services in the energy and ancillary services co-optimized markets [10]. In a low renewable energy penetrated system, demand is the major source of real time uncertainty and variability. Consequently, this mechanism might work efficiently. However, in a high wind power penetration system, wind power brings additional significant ancillary services requirements. How to allocate the ancillary services cost, such as flexible ramping products costs, among demand and wind power to improve the fairness and efficiency of the market operation is an urgent issue.

In Ref. [11], [12], a security constrained unit commitment model was proposed based on chance constrained (CC) optimization to consider the wind power uncertainty. In [13]— [15], the chance constrained optimization was applied in the AC OPF problems to maintain the system security considering the uncertain renewable power output. In Ref. [16]-[18], distributionally robust CC-OPF models have been studied to mitigate the uncertainties in system operation. In these previous studies, the FRPs were not explicitly considered and priced. In addition, the chance constraints in these studies deployed a symmetric affine policy (SAP) which required the generators to respond symmetrically under the negative and positive system imbalance conditions. To address the aforementioned issues in the current FRPs modeling, a distributionally-robust chance constrained multi-interval OPF (DRCC-MIOPF) model is proposed. The flexible ramping requirements are endogenously

modeled considering the spatiotemporal correlation of wind power outputs and demand. The impacts of FRPs are considered in all of the system security constraints, such as generation capacity limitations, ramping capability and the transmission constraints. Therefore, the delivery of FRPs in the real time operation is guaranteed. Furthermore, different from the previous SAP model, an asymmetrical affine policy (AAP) is proposed to leverage the flexibility of generators to mitigate the system uncertainty in different directions, which increases the system operational flexibility and reduces the operating cost. Finally, the prices of FRPs are derived from the proposed AAP-DRCC-MIOPF model to allocate the FRPs costs to the uncertainty sources and compensate the controllable generation resources providing the FRPs. The main contributions of this paper can be summarized as follows:

- 1) Deliverable FRPs have been proposed to guarantee the delivery of the FRPs in real time operation.
- 2) The spatiotemporal correlation of demand and wind power uncertainties has been considered in the FRPs model which evaluates the system ramping requirements accurately.
- 3) An asymmetrical affine policy (AAP) is adopted to deploy the generation flexibility to mitigate the uncertainties in different directions to reduce the costs.
- 4) An uncertainty-contained locational marginal price (U\_LMP) mechanism is proposed and decomposed to price the FRPs for the uncertain demand and wind power.
- The FRPs cost is allocated based on the actual demand and wind power ramping requirements because of their variability instead of a heuristic allocation mechanism.

The rest of this paper is organized as follows: Section II presents the spatiotemporal correlation in the FRPs modeling; Section III proposes the asymmetrical affine policy (AAP) based distributionally-robust chance constrained multi-interval OPF (AAP-DRCC-MIOPF) model; Section IV derives the prices of FRPs from the proposed AAP-DRCC-MIOPF model; Section V performs the case studies on the PJM 5-bus, IEEE 39-bus and IEEE 118-bus systems to validate the proposed method; and Section VI concludes the paper.

# II. FLEXIBLE RAMPING PRODUCTS WITH SPATIOTEMPORAL CORRELATION

In the system RTED, FRPs mitigate the system demand and wind power forecast uncertainties. In this process, the temporal correlation between adjacent time intervals should be considered. For example, when the temporal correlation is positive, the variation directions of two intervals' power are likely to be the same. This leads to a lower ramping requirement. In contrast, if the temporal correlation is negative, the variation directions of two intervals' power are likely to be opposite, which requires a higher ramping capability.

The effect of the spatiotemporal correlation on the ramping requirement is demonstrated using four Gaussian distributed random variables (representing the power outputs of two demands at two consecutive time intervals), for the sake of illustration. Other distributions have a similar observation which can be demonstrated using numerical simulation. Consider the ramping random variable  $R_t$  defined by:

$$R_t = V_{1,t} + V_{2,t} - V_{1,t-1} - V_{2,t-1}$$
 (1)

where  $V_{1,t}$ ,  $V_{2,t}$ ,  $V_{1,t-1}$  and  $V_{2,t-1}$  represent four Gaussian distributed random variables such as two demands (demand 1 and 2) at two intervals t and t-1. The explicit formulation of  $R_t$ is given by [19]:

$$R_{t} \sim N(E(V_{1,t}) + E(V_{2,t}) - E(V_{1,t-1}) - E(V_{2,t-1}), \sigma_{1,t}^{2} + \sigma_{2,t}^{2} + \sigma_{1,t-1}^{2} + \sigma_{2,t-1}^{2} + 2\gamma_{t}\sigma_{1,t}\sigma_{2,t} + 2\gamma_{t-1}\sigma_{1,t-1}\sigma_{2,t-1} - 2\rho_{1}\sigma_{1,t}\sigma_{1,t-1} - 2\rho_{2}\sigma_{2,t}\sigma_{2,t-1})$$

$$(2)$$

where  $E(\cdot)$  represents the expectation of random variables;  $\rho_1$ and  $\rho_2$  are the temporal correlation between two intervals of two demands, respectively;  $\gamma_t$  and  $\gamma_{t-1}$  represent the spatial correlation between two demands at two intervals. From the formulation in Eq. (2), it is obvious that the variation range of  $R_t$  is determined by not only the variation of two intervals random variables, but also their spatiotemporal correlation. Ignoring this spatiotemporal correlation can lead to overestimates/underestimates of ramping requirements.

Similarly, if  $V_t$  is the net-demand, i.e., the demand minus wind power, then similarly  $R_t$  in Eq. (2) are decided by not only the variation of individual demand at each interval, but also the spatiotemporal correlations of wind power plants (WPPs) and demands. Therefore, the spatiotemporal correlation of both WPPs and demands should be taken into consideration in the FRPs modeling.

#### III. AAP BASED CHANCE-CONSTRAINED MIOPF

## A. Asymmetrical Affine Policy for Forecast Uncertainty

In previous CC-OPF research, a SAP was used to determine the corrective control of generators for the renewable and demand power forecast uncertainty [15]-[17], [20]. The main advantages of the SAP are that the generator's output change depends linearly on the forecast errors regardless of the uncertainty direction. However, in the SAP, the generators' upward and downward responses are symmetrical which restricts the generation resources from providing the corrective control when their power output is at their upper or lower limits, as illustrated in Fig. 1 (SAP case). In fact, in the SAP case, once the output G drops to its minimum  $G_{min}$ ,  $\Delta G_D$  (the downward response) becomes zero and because of the symmetric nature of the SAP approach,  $\Delta G_U$  (the upward response) is forced to zero as well.

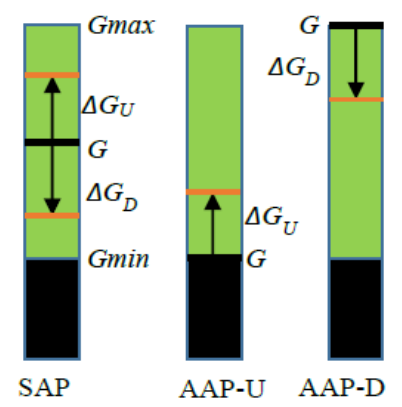


Fig. 1 Illustration of SAP and AAP

However, when the generator's power output is at the upper limit, it still can provide the downward response and the generators at the lower limit can provide the upward response. Consequently, the solutions from the SAP model might be suboptimal. In [21], a linear weight and piece-wise affine policy for generators' corrective control was proposed to differentiate the small and large system deviations. In this policy, the generators' corrective control was still symmetrical within the small deviation range. The generators control action was not differentiated based on the system imbalance directions.

To fully leverage the generation's flexibility, an AAP for the forecast uncertainty is adopted. The flexibility of generators will be deployed in an improved manner as shown in Fig. 1 (AAP cases).

The SAP based corrective control is represented in Eq. (3).

$$G_{i,t} = G_{exp,i,t} + \boldsymbol{\beta}_{i,t}^T \boldsymbol{u_t}$$
 (3)

The proposed AAP based corrective control dissociates upward and downward balancing responses as in (4) and (5).

$$G_{i,t} = G_{exp,i,t} + \boldsymbol{\beta}_{U,i,t}^T \boldsymbol{u}_t, \text{ if } \mathbf{1}^T \widetilde{\boldsymbol{u}_t} > 0$$
(4)

$$G_{i,t} = G_{exp,i,t} + \boldsymbol{\beta}_{D,i,t}^T \boldsymbol{u}_t, \text{ if } \mathbf{1}^T \widetilde{\boldsymbol{u}_t} \le 0$$
 (5)

where  $u_t$  represents the uncertainty of demand and wind power forecast at time t;  $\beta_{i,t}^T$  is the balancing factor in the SAP model;  $\widetilde{u_t}$  is the realized system imbalance including the demand and wind power forecast errors;  $\beta_{U,i,t}^T$  and  $\beta_{D,i,t}^T$  are the balancing factor for the up/down response in the proposed AAP model.

#### B. AAP based CC-MIOPF

When the wind power and demand forecast uncertainties  $(\Delta P_{i,t} \text{ and } \Delta D_{i,t})$  are considered, the generation output is shown in Eq. (6), including a corrective response component  $\Delta G_{i.t.}$ 

$$G_{i,t} = G_{exp,i,t} + \Delta G_{i,t} \tag{6}$$

$$P_{i,t} = P_{exp,i,t} + \Delta P_{i,t} \tag{7}$$

$$D_{i,t} = D_{exp,i,t} + \Delta D_{i,t} \tag{8}$$

$$\Delta G_{U,i,t} = \beta_{U,i,t} \left( -\sum_{i=1}^{N} \Delta P_{i,t} + \sum_{i=1}^{N} \Delta D_{i,t} \right)$$
 (9)

$$\sum_{i=1}^{N} \beta_{U,i,t} = 1 \tag{10}$$

$$\Delta G_{D,i,t} = \beta_{D,i,t} \left( -\sum_{i=1}^{N} \Delta P_{i,t} + \sum_{i=1}^{N} \Delta D_{i,t} \right)$$
(11)

$$\sum_{i=1}^{N} \beta_{D,i,t} = 1 \tag{12}$$

Because the formulation of  $\Delta G_{U,i,t}$  and  $\Delta G_{D,i,t}$  are the same except using the  $\beta_{U,i,t}$  and  $\beta_{D,i,t}$  respectively, in the following text, the U and D subscripts are omitted in several equations to make the model description concise. The uncertainty components in the following text with U in the subscript means that it is calculated with  $\beta_{U,i,t}$ . The uncertainty components with D in the subscript means that it is calculated with  $\beta_{D,i,t}$ .

In this paper, the total generation cost at different intervals is minimized, as shown in Eq. (13a). We study the system dispatch over a one-hour period comprising T = 12 fiveminute intervals. Thus, the CC-MIOPF model is to minimize the generation cost of forecasted demand and wind power.

$$\min f_{exp} = \sum_{t \in T} \left( \sum_{i=1}^{N} c_{i,t} G_{exp,i,t} \right)$$
 (13a)

s.t. 
$$\sum_{i=1}^{N} (G_{i,t} + P_{i,t}) - \sum_{i=1}^{N} D_{i,t} = 0: \lambda_t, \forall t \in \{1, \dots, T\}$$
 (13b)  
 $\Pr(\sum_{i=1}^{N} GSF_{l,i}(G_{i,t} + P_{i,t} - D_{i,t}) \le LU_l) \ge 1 - \epsilon, \forall t \in$ 

$$(\sum_{i=1}^{r} GSF_{l,i}(G_{i,t} + P_{i,t} - D_{i,t}) \le LU_l) \ge 1 - \epsilon, \forall t \in \{1, \dots, T\}, \forall l \in Lines \quad (13c)$$

$$Pr(\sum_{i=1}^{N} GSF_{l,i}(G_{i,t} + P_{i,t} - D_{i,t}) \leq LO_{l}) \geq 1 - \epsilon, \forall t \in \{1, \dots, T\}, \forall l \in Lines \quad (13c)$$

$$Pr(\sum_{i=1}^{N} GSF_{l,i}(G_{i,t} + P_{i,t} - D_{i,t}) \geq -LU_{l}) \geq 1 - \epsilon, \forall t \in \{1, \dots, T\}, \forall l \in Lines \quad (13d)$$

$$\Pr(G_{i,t} \le G_i^{max}) \ge 1 - \epsilon, \forall t \in \{1, \dots, T\}, \forall i \in Gen$$
 (13e)

$$\Pr(G_i^{min} \le G_{i,t}) \ge 1 - \epsilon, \forall t \in \{1, \dots, T\}, \forall i \in Gen$$
 (13f)

 $\begin{aligned} & \mathbf{Pr} \big( G_{i,t} - G_{i,t-1} \leq R_i^U \cdot \Delta t \big) \geq 1 - \epsilon, \forall t \in \{2, \cdots, T\}, \forall \ i \in Gen(13g) \\ & \mathbf{Pr} \big( G_{i,t-1} - G_{i,t} \leq R_i^D \cdot \Delta t \big) \geq 1 - \epsilon, \forall t \in \{2, \cdots, T\}, \forall \ i \in Gen(13h) \end{aligned}$ where (13c)–(13h) represent the chance constraints considering the impacts of wind power and demand forecast uncertainties on the violation probabilities of power flow limits, generation upper/lower limitation, and generation ramping capability.  $\lambda_t$  is the dual variable associated with the power balance constraint.

Considering the uncertainties of demand and wind power outputs, the power flow uncertainty can be formulated with a combination of demand and wind power uncertainties. First, assume that the uncertain part of the wind power output  $\Delta P$  has **0** mean and the covariance matrix as  $\Sigma_{w,t}$  for every time interval shown in Eq (17) [13], [18]. The uncertain part of demand  $\Delta D$ has a **0** mean and the covariance  $\Sigma_{d,t}$  shown in Eq. (18). The standard deviation of the random power flow is below.

$$\sigma_{PF.l.t} =$$

$$\sqrt{a_{l,w,t}(\boldsymbol{\beta_t})^T \boldsymbol{\Sigma_{w,t}} a_{l,w,t}(\boldsymbol{\beta_t}) + a_{l,d,t}(\boldsymbol{\beta_t})^T \boldsymbol{\Sigma_{d,t}} a_{l,d,t}(\boldsymbol{\beta_t})}$$
 (14) where  $a_{l,w,t}(\boldsymbol{\beta_t})$  and  $a_{l,d,t}(\boldsymbol{\beta_t})$  are a one-column matrix with the *i*-th element as shown in Eq. (15) and (16):

$$a_{l,i,w,t}(\boldsymbol{\beta_t}) = -\sum_{k=1}^{N} GSF_{l,k} \, \beta_{k,t} + GSF_{l,i}$$
 (15)

$$a_{l,i,d,t}(\boldsymbol{\beta_t}) = \sum_{k=1}^{N} GSF_{l,k} \, \beta_{k,t} - GSF_{l,i}$$
 (16)

$$\Sigma_{w,t} = \begin{bmatrix} \sigma_{w,t,1}^2 & \rho_{w,1,2}\sigma_{w,t,1}\sigma_{w,t,2} \\ \rho_{w,1,2}\sigma_{w,t,1}\sigma_{w,t,2} & \sigma_{w,t,2}^2 \end{bmatrix}$$
(17)

$$a_{l,i,w,t}(\boldsymbol{\beta_t}) = -\sum_{k=1}^{N} dSF_{l,k} \, \beta_{k,t} + dSF_{l,i}$$

$$a_{l,i,d,t}(\boldsymbol{\beta_t}) = \sum_{k=1}^{N} GSF_{l,k} \, \beta_{k,t} - GSF_{l,i}$$

$$\boldsymbol{\Sigma}_{w,t} = \begin{bmatrix} \sigma_{w,t,1}^2 & \rho_{w,1,2}\sigma_{w,t,1}\sigma_{w,t,2} \\ \rho_{w,1,2}\sigma_{w,t,1}\sigma_{w,t,2} & \sigma_{w,t,2}^2 \end{bmatrix}$$

$$\boldsymbol{\Sigma}_{d,t} = \begin{bmatrix} \sigma_{d,t,1}^2 & \rho_{d,1,2}\sigma_{d,t,1}\sigma_{d,t,2} \\ \rho_{d,1,2}\sigma_{d,t,1}\sigma_{d,t,2} & \sigma_{d,t,2}^2 \end{bmatrix}$$

$$(18)$$

where  $\rho_{w,1,2}$  and  $\rho_{d,1,2}$  are the spatial correlation of WPPs, and demand illustrated with two demands and two WPPs, respectively.

Therefore, the AAP based chance constraints of (13c) and (13d) can be reformulated [22] as:

$$\sum_{i=1}^{N} \left[ GSF_{l,i} \left( G_{exp,i,t} + P_{exp,i,t} - D_{exp,i,t} \right) \right] + K_{\epsilon} \sigma_{PF,U,l,t} \le LU_{l}$$
(19)

$$\sum_{i=1}^{N} \left[ GSF_{l,i} \left( G_{exp,i,t} + P_{exp,i,t} - D_{exp,i,t} \right) \right] - K_{\epsilon} \sigma_{PF,U,l,t} \ge -LU_{l}$$
(20)

$$\sum_{i=1}^{N} \left[ GSF_{l,i} \left( G_{exp,i,t} + P_{exp,i,t} - D_{exp,i,t} \right) \right] + K_{\epsilon} \sigma_{PF,D,l,t} \le LU_{l}$$
(21)

$$\sum_{i=1}^{N} \left[ GSF_{l,i} \left( G_{exp,i,t} + P_{exp,i,t} - D_{exp,i,t} \right) \right] - K_{\epsilon} \sigma_{PF,D,l,t} \ge -LU_{l}$$
 (22)

where  $\sigma_{PF,U,l,t}$  and  $\sigma_{PF,D,l,t}$  are calculated using Eq. (14) with  $\beta_{U,i,t}$  and  $\beta_{D,i,t}$  respectively;  $K_{\epsilon}$  is the coefficient to control the robustness of the forecast errors in the chance constraints, which will be explained in the next subsection.

The generators' limits in AAP-based chance constraints are illustrated in Fig. 2. In (13e) and (13f), the standard deviation of the generation output is below.

$$\sigma_{g,i,t} = \sqrt{\boldsymbol{b}_{w,i,t}(\boldsymbol{\beta}_t)^T \boldsymbol{\Sigma}_{w,t} \boldsymbol{b}_{w,i,t}(\boldsymbol{\beta}_t) + \boldsymbol{b}_{d,i,t}(\boldsymbol{\beta}_t)^T \boldsymbol{\Sigma}_{d,t} \boldsymbol{b}_{d,i,t}(\boldsymbol{\beta}_t)}$$
(23)

where  $\sigma_{q,i}$  represents the random generation corrective response, and  $b_i(\beta_t)$  is a one-column matrix with the elements

$$\boldsymbol{b}_{w,i,t}(\boldsymbol{\beta}_t) = \underbrace{[-\beta_{i,t} \quad \cdots \quad -\beta_{i,t}]^T}_{NW}$$
(24)

$$\mathbf{b}_{w,i,t}(\boldsymbol{\beta_t}) = \underbrace{[-\beta_{i,t} \quad \cdots \quad -\beta_{i,t}]^T}_{NW}$$

$$\mathbf{b}_{d,i,t}(\boldsymbol{\beta_t}) = \underbrace{[\beta_{i,t} \quad \cdots \quad \beta_{i,t}]^T}_{ND}$$
(24)

where NW and ND are the numbers of WPPs and demand.

Then (13e) and (13f) can be reformulated as:

$$G_{i,t} + K_{\epsilon} \sigma_{g,U,i,t} \le G_i^{max} \tag{26}$$

$$G_{i,t} - K_{\epsilon} \sigma_{q,D,i,t} \ge G_i^{min} \tag{27}$$

where  $\sigma_{U,g,i,t}$  and  $\sigma_{D,g,i,t}$  are calculated using Eq. (23) with  $\beta_{U,i,t}$  and  $\beta_{D,i,t}$  in Eq. (24) and (25) respectively; the equality constraints in (14) and (23) can be reformulated as second order cone (SOC) constraints as below by introducing the auxiliary variables  $\eta_{PF,U,l,t}$ ,  $\eta_{PF,D,l,t}$ ,  $\eta_{g,U,i,t}$ , and  $\eta_{g,D,i,t}$ .

$$\left\| \begin{bmatrix} \boldsymbol{\Sigma}_{w,t}^{1/2} & \\ & \boldsymbol{\Sigma}_{d,t}^{1/2} \end{bmatrix} \begin{bmatrix} \boldsymbol{a}_{l,w,t}(\boldsymbol{\beta}_{U,t}) \\ \boldsymbol{a}_{l,d,t}(\boldsymbol{\beta}_{U,t}) \end{bmatrix} \right\|_{2} \leq \eta_{PF,U,l,t} : \vartheta_{U,l,t}$$
 (28)

variables 
$$\eta_{PF,U,l,t}$$
,  $\eta_{PF,D,l,t}$ ,  $\eta_{g,U,i,t}$ , and  $\eta_{g,D,i,t}$ .

$$\left\|\begin{bmatrix} \Sigma_{w,t}^{1/2} & \\ & \Sigma_{d,t}^{1/2} \end{bmatrix} \begin{bmatrix} a_{l,w,t}(\boldsymbol{\beta}_{U,t}) \\ a_{l,d,t}(\boldsymbol{\beta}_{U,t}) \end{bmatrix}\right\|_{2} \leq \eta_{PF,U,l,t} : \vartheta_{U,l,t} \qquad (28)$$

$$\left\|\begin{bmatrix} \Sigma_{w,t}^{1/2} & \\ & \Sigma_{d,t}^{1/2} \end{bmatrix} \begin{bmatrix} a_{l,w,t}(\boldsymbol{\beta}_{D,t}) \\ a_{l,d}, t(\boldsymbol{\beta}_{D,t}) \end{bmatrix}\right\|_{2} \leq \eta_{PF,D,l,t} : \vartheta_{D,l,t} \qquad (29)$$

$$\left\|\begin{bmatrix} \Sigma_{w,t}^{1/2} & \\ & \Sigma_{d,t}^{1/2} \end{bmatrix} \begin{bmatrix} b_{w,i,t}(\boldsymbol{\beta}_{U,t}) \\ b_{d,i,t}(\boldsymbol{\beta}_{U,t}) \end{bmatrix}\right\|_{2} \leq \eta_{g,U,i,t} : \vartheta_{g,U,i,t} \qquad (30)$$

$$\left\|\begin{bmatrix} \Sigma_{w,t}^{1/2} & \\ & \Sigma_{d,t}^{1/2} \end{bmatrix} \begin{bmatrix} b_{w,i,t}(\boldsymbol{\beta}_{D,t}) \\ b_{d,i,t}(\boldsymbol{\beta}_{D,t}) \end{bmatrix}\right\|_{2} \leq \eta_{g,D,i,t} : \vartheta_{g,D,i,t} \qquad (31)$$
where  $\vartheta_{u,u,t}$  and  $\vartheta_{u,u,t}$  are the dual variables

$$\left\| \begin{bmatrix} \boldsymbol{\Sigma}_{w,t}^{1/2} & \\ & \boldsymbol{\Sigma}_{d,t}^{1/2} \end{bmatrix} \begin{bmatrix} \boldsymbol{b}_{w,i,t}(\boldsymbol{\beta}_{U,t}) \\ \boldsymbol{b}_{d,i,t}(\boldsymbol{\beta}_{U,t}) \end{bmatrix} \right\|_{2}^{2} \leq \eta_{g,U,i,t} : \theta_{g,U,i,t}$$
 (30)

$$\left\| \begin{bmatrix} \boldsymbol{\Sigma}_{w,t}^{1/2} & \\ & \boldsymbol{\Sigma}_{d,t}^{1/2} \end{bmatrix} \begin{bmatrix} \boldsymbol{b}_{w,i,t}(\boldsymbol{\beta}_{D,t}) \\ \boldsymbol{b}_{d,i,t}(\boldsymbol{\beta}_{D,t}) \end{bmatrix} \right\|_{2} \leq \eta_{g,D,i,t} : \theta_{g,D,i,t}$$
(31)

where  $\theta_{U,l,t}$ ,  $\theta_{D,l,t}$ ,  $\theta_{g,U,i,t}$ , and  $\theta_{g,D,i,t}$  are the dual variables associated with the constraints on the left side of the colons.

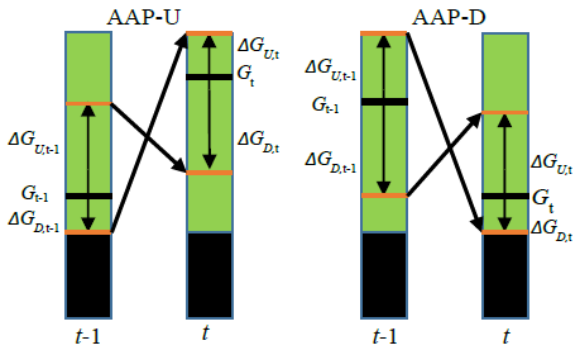


Fig. 2 Generation limitation under AAP

For the generation ramping constraints in (13g) and (13h), the AAP-based ramping up and down chance constraints can be formulated as below as shown in Fig. 2.

$$Ramp_{i,t}^{U} = G_{exp,i,t} + \Delta G_{i,t}^{U} - G_{exp,i,t-1} - \Delta G_{i,t-1}^{D}$$
 (32)

$$Ramp_{i,t}^{D} = G_{exp,i,t-1} + \Delta G_{i,t-1}^{U} - G_{exp,i,t} - \Delta G_{i,t}^{D}$$
 (33)

$$Ramp_{i,t}^{U} = G_{exp,i,t} + \Delta G_{i,t}^{U} - G_{exp,i,t-1} - \Delta G_{i,t-1}^{D}$$
(32)  

$$Ramp_{i,t}^{D} = G_{exp,i,t-1} + \Delta G_{i,t-1}^{U} - G_{exp,i,t} - \Delta G_{i,t}^{D}$$
(33)  

$$\left\| \begin{bmatrix} \Xi_{w,t}^{1/2} \\ \Xi_{d,t}^{1/2} \end{bmatrix} \begin{bmatrix} B_{U,w,i,t}(\boldsymbol{\beta}_{t}) \\ B_{U,d,i,t}(\boldsymbol{\beta}_{t}) \end{bmatrix} \right\|_{2} \leq r_{g,U,i,t} : \varphi_{U,i,t}$$
(34)

$$\boldsymbol{B}_{U,w,i,t}(\boldsymbol{\beta}_t) = [-\boldsymbol{b}_{w,i,t-1}(\boldsymbol{\beta}_{D,t}) \quad \boldsymbol{b}_{w,i,t}(\boldsymbol{\beta}_{U,t})]^T$$
(35)

$$\boldsymbol{B}_{U,d,i,t}(\boldsymbol{\beta}_t) = [-\boldsymbol{b}_{d,i,t-1}(\boldsymbol{\beta}_{D,t}) \quad \boldsymbol{b}_{d,i,t}(\boldsymbol{\beta}_{U,t})]^T$$
(36)

$$\left\| \begin{bmatrix} \Xi_{w,t}^{1/2} & \\ & \Xi_{d,t}^{1/2} \end{bmatrix} \begin{bmatrix} B_{D,w,i,t}(\boldsymbol{\beta_t}) \\ B_{D,d,i,t}(\boldsymbol{\beta_t}) \end{bmatrix} \right\|_{2} \le r_{g,D,i,t} : \varphi_{D,i,t}$$
(37)

$$\boldsymbol{B}_{D,w,i,t}(\boldsymbol{\beta}_t) = [\boldsymbol{b}_{w,i,t-1}(\boldsymbol{\beta}_{U,t}) \quad -\boldsymbol{b}_{w,i,t}(\boldsymbol{\beta}_{D,t})]^T$$
(38)

$$\boldsymbol{B}_{D,d,i,t}(\boldsymbol{\beta}_t) = [\boldsymbol{b}_{d,i,t-1}(\boldsymbol{\beta}_{U,t}) \quad -\boldsymbol{b}_{d,i,t}(\boldsymbol{\beta}_{D,t})]^T$$
(39)

$$\Xi_{w,t} = \begin{bmatrix} \Sigma_{w,t-1} & \Sigma_{w,t-1,t} \\ \Sigma_{w,t+1} & \Sigma_{w,t} \end{bmatrix}$$
(40)

$$B_{D,w,i,t}(\mathbf{p}_{t}) = [b_{w,t,t-1}(\mathbf{p}_{t,t}) \quad b_{w,t,t}(\mathbf{p}_{t}), t]$$

$$B_{D,d,i,t}(\boldsymbol{\beta}_{t}) = [b_{d,i,t-1}(\boldsymbol{\beta}_{U,t}) \quad -b_{d,i,t}(\boldsymbol{\beta}_{D,t})]^{T}$$

$$\Xi_{w,t} = \begin{bmatrix} \Sigma_{w,t-1} & \Sigma_{w,t-1,t} \\ \Sigma_{w,t,t-1} & \Sigma_{w,t} \end{bmatrix}$$

$$\Xi_{d,t} = \begin{bmatrix} \Sigma_{d,t-1} & \Sigma_{d,t-1,t} \\ \Sigma_{d,t,t-1} & \Sigma_{d,t} \end{bmatrix}$$

$$(41)$$

Note that in (35) and (36), the balancing factor for the interval t-1 is  $\beta_{D,t}$  and for the interval t is  $\beta_{U,t}$  for the up ramp. In contrast, the balancing factor for t-1 is  $\beta_{U,t}$  and for t is  $\beta_{D,t}$ for the down ramp in (38) and (39). This is illustrated in Fig. 2.

In (40) and (41), the covariance matrix components are listed

below. 
$$\Sigma_{w,t-1,t} = \begin{bmatrix} \gamma_{w1,t-1,t} \sigma_{w1,t-1} \sigma_{w1,t} & 0 \\ 0 & \gamma_{w2,t-1,t} \sigma_{w2,t-1} \sigma_{w2,t} \end{bmatrix} (42)$$

$$\Sigma_{w,t,t-1} = \begin{bmatrix} \gamma_{w1,t,t-1} \sigma_{w1,t} \sigma_{w1,t-1} & 0 \\ 0 & \gamma_{w2,t-1,t} \sigma_{w2,t-1} \sigma_{w2,t} \end{bmatrix} (43)$$

$$\Sigma_{d,t-1,t} = \begin{bmatrix} \gamma_{d1,t-1,t} \sigma_{d1,t-1} \sigma_{d1,t} & 0 \\ 0 & \gamma_{d2,t-1,t} \sigma_{d2,t-1} \sigma_{d2,t} \end{bmatrix} (44)$$

$$\Sigma_{d,t,t-1} = \begin{bmatrix} \gamma_{d1,t,t-1} \sigma_{d1,t} \sigma_{d1,t-1} & 0 \\ 0 & \gamma_{d2,t-1,t} \sigma_{d2,t-1} \sigma_{d2,t} \end{bmatrix} (45)$$
where  $\gamma_{w,t-1,t}$  and  $\gamma_{d,t-1,t}$  are temporal correlation of WPPs

where  $\gamma_{w,t-1,t}$  and  $\gamma_{d,t-1,t}$  are temporal correlation of WPPs and demands;  $\Sigma_{w,t,t-1}$  and  $\Sigma_{w,t-1,t}$  are the covariance matrixes of the WPPs forecast errors between intervals t-1 and t including the temporal correlation;  $\Sigma_{w,t-1}$  and  $\Sigma_{w,t}$  in Eq. (40) are from Eq. (17).

Then, the AAP-based CC-MIOPF model is formulated as: min  $f_{exp}$ (46a) s.t. Constraints (10), (12), (15)-(18), (24), (25), (28)-(31), (46b)(34)-(45) $\sum_{i=1}^{N} (G_{exp,i,t} + P_{exp,i,t}) - \sum_{i=1}^{N} D_{exp,i,t} = 0: \lambda_{t}$ (46c) $\sum_{i=1}^{N} \left[ GSF_{l,i} \left( G_{exp,i,t} + P_{exp,i,t} - D_{exp,i,t} \right) \right] + K_{\epsilon} \eta_{PF,U,l,t} \le \max_{max} \left[ \frac{1}{2} \left( \frac{1}{2} \left($ (46d)
$$\begin{split} \sum_{i=1}^{N} \left[ GSF_{l,i} \left( G_{exp,i,t} + P_{exp,i,t} - D_{exp,i,t} \right) \right] - K_{\epsilon} \eta_{PF,U,l,t} \geq \\ - LU_{l} : \mu_{l,U,t}^{min} \end{split}$$
 $\sum_{i=1}^{N} \left[ GSF_{l,i} \left( G_{exp,i,t} + P_{exp,i,t} - D_{exp,i,t} \right) \right] + K_{\epsilon} \eta_{PF,D,l,t} \leq LU_{l} : \mu_{l,D,t}^{max}$ (46e)

$$\sum_{i=1}^{N} \left[ GSF_{l,i} \left( G_{exp,i,t} + P_{exp,i,t} - D_{exp,i,t} \right) \right] - K_{\epsilon} \eta_{PF,D,l,t} \ge -LU_{l} : \mu_{l,D,t}^{min} \qquad (46g)$$

$$G_{exp,i,t} + K_{\epsilon} \eta_{g,U,i,t} \le G_i^{max} : \omega_{i,t}^{max}$$

$$G_{exp,i,t} - K_{\epsilon} \eta_{g,D,i,t} \ge G_i^{min} : \omega_{i,t}^{min}$$

$$\tag{46i}$$

$$G_{exn,i,t} - K_{\epsilon} \eta_{a,D,i,t} \ge G_i^{min} : \omega_{i,t}^{min}$$
 (46i)

$$G_{exp,i,t} - G_{exp,i,t-1} + K_{\epsilon} r_{g,U,i,t} \le R_i^U \cdot \Delta t : \tau_{i,t}^{max}$$

$$\tag{46j}$$

$$G_{exp,i,t} - G_{exp,i,t-1} - K_{\epsilon} r_{g,p,i,t} \ge -R_i^D \cdot \Delta t; \tau_{i,t}^{min}$$

$$(46k)$$

where the variables on the right side of the colons are the dual variables of the constraints on the left side of the colons.

## C. Distributionally-Robust Model

Although the Gaussian distribution is used to illustrate the spatiotemporal correlation in Section II, in the chance constrained formulation, the distribution is not predetermined for the forecast uncertainties of demand and wind power. Using only the mean  $\hat{\mu}$  and covariance  $\Xi$  obtained from the historical forecast errors data, for  $\epsilon \in (0,1)$ , the distributionally-robust chance constrained (DRCC) model is determined with the value of  $K_{\epsilon}$  decided by Eq. (47)

$$K_{\epsilon} = \sqrt{(1 - \epsilon)/\epsilon} \tag{47}$$

If the forecast error distribution is assumed to be symmetrical, the model is formulated [22] with the value of  $K_{\epsilon}$ :

$$K_{\epsilon} = \sqrt{1/2\epsilon} \tag{48}$$

The proof for Eq. (47) and (48) is in [22]. The values of  $K_{\epsilon}$ in the symmetrically distributionally-robust case (Sym. Dist. R.), the distributionally-robust case (Dist. R.), and Gaussian distribution case are 3.1623, 4.3589, and 1.645, when  $\epsilon$  is 5%

#### IV. PRICING MODEL OF FLEXIBLE RAMPING PRODUCTS

After obtaining the multi-interval generation scheduling solution considering the flexible ramping requirements, it is important to obtain the financial settlement, i.e. who should pay how much for the FRPs and how to compensate the controllable resources providing the FRPs.

In the current FRPs design, the energy, FRPs and other ancillary services are co-optimized and an explicit FRPs requirements constraint is modeled [1], [2]. Therefore, the shadow prices of the FRPs requirement constraints are employed to derive the FRPs prices, which reflect the coupled effects of the generation schedule and FRPs and other ancillary services schedules. However, in the proposed model in this paper, there is no explicit FRPs requirement constraints. The FRPs are procurement endogenously considering the uncertainty of demand and variable generation at different time intervals. Although it has the aforementioned deliverability advantages over the traditional FRPs procurement, it also brings new challenges for FRPs price derivation. Current ancillary services pricing approaches [24], [25] cannot be used due to the lack of explicit FRPs requirement constraints.

In this paper, an uncertainty contained LMP (U LMP) model is proposed to settle the FRPs. To obtain the U LMP for the uncertain demand and wind power, the Lagrangian function of the model (46) is first formulated. Please refer to APPENDIX Eq. (A1) for details. Then the U LMP for the demand at Bus i considering its uncertainty is derived from the Lagrangian function in (A1) as shown in APPENDIX Eq. (A2). After that, the U LMP can be decomposed into several components similar to the current LMP formulation in Eq (49), where (52)-(54) are the uncertainty components.

If  $\vartheta_{U,l,t}$  is larger than 0, Constraint (28) is binding, and the

following equality in Eq. (52) holds:
$$\eta_{PF,U,l,t} = \left\| \begin{bmatrix} \boldsymbol{\Sigma}_{w,t}^{1/2} \\ \boldsymbol{\Sigma}_{d,t}^{1/2} \end{bmatrix} \begin{bmatrix} \boldsymbol{a}_{l,w,t}(\boldsymbol{\beta}_{U,t}) \\ \boldsymbol{a}_{l,d,t}(\boldsymbol{\beta}_{U,t}) \end{bmatrix} \right\|_{2}$$
(50)

And when  $\vartheta_{U,l,t} = 0$ , Constraint (28) is an inequality constraint as in Eq. (53)

$$\eta_{PF,U,l,t} > \left\| \begin{bmatrix} \Sigma_{w,t}^{1/2} \\ & \Sigma_{d,t}^{1/2} \end{bmatrix} \begin{bmatrix} a_{l,w,t}(\boldsymbol{\beta}_{U,t}) \\ a_{l,d,t}(\boldsymbol{\beta}_{U,t}) \end{bmatrix} \right\|_{2}$$
 (51)

Similar relationships can be applied to other SOC constraints and their dual variables in Eq. (29)-(31) and Eq. (34), (37). Consequently, the uncertainty components of U LMP are formulated as Eq. (52) to (54).

$$U_{-}LMP_{Load,i,t} = \frac{\partial L(x)}{\partial D_{exp,i,t}} = \lambda_t + \sum_{l=1}^{M} GSF_{l,i} \left( \mu_{l,U,t}^{min} - \mu_{l,U,t}^{max} + \mu_{l,D,t}^{min} - \mu_{l,D,t}^{max} \right) + U_{-}LMP_{-}PF_{Load,i,t} + U_{-}LMP_{-}G_{Load,i,t} + U_{-}LMP_{-}G_{Load,i,t}$$

$$(49)$$

(46f)

$$U_{-}LMP_{-}PF_{Load,i,t} = \sum_{l=1}^{M} \vartheta_{U,l,t} \frac{a_{l-i,d,t}(\beta_{U,t})\xi_{d,i,t}\sum_{j=1}^{ND} \rho_{d,i,j}a_{l-j,d,t}(\beta_{U,t})\xi_{d,j,t}D_{exp,j,t}}{\eta_{PF,U,l,t}} + \sum_{l=1}^{M} \vartheta_{D,l,t} \frac{a_{l-i,d,t}(\beta_{D,t})\xi_{d,i,t}\sum_{j=1}^{ND} \rho_{d,i,j}a_{l-j,d,t}(\beta_{D,t})\xi_{d,j,t}D_{exp,j,t}}{\eta_{PF,D,l,t}}$$
(52)

$$U_{LMP}G_{Load,i,t} = \sum_{j=1}^{N} \theta_{g,U,j,t} \frac{\beta_{U,j,t} \xi_{d,i,t} \sum_{k=1}^{ND} \rho_{d,i,k} \beta_{U,j,t} \xi_{d,k,t} D_{exp,k,t}}{\eta_{g,U,j,t}} + \sum_{j=1}^{N} \theta_{g,D,j,t} \frac{\beta_{D,j,t} \xi_{d,i,t} \sum_{k=1}^{ND} \rho_{d,i,k} \beta_{D,j,t} \xi_{d,k,t} D_{exp,k,t}}{\eta_{g,D,j,t}}}{\eta_{g,D,j,t}} + \sum_{j=1}^{N} \theta_{g,D,j,t} \frac{\beta_{D,j,t} \xi_{d,i,t} \sum_{k=1}^{ND} \rho_{d,i,k} \beta_{D,j,t} \xi_{d,k,t} D_{exp,k,t}}{\eta_{g,D,j,t}}}{r_{g,U,j,t}} + \sum_{j=1}^{N} \phi_{D,j,t} \frac{\gamma_{d,i,t,t-1} \beta_{D,j,t} \xi_{d,i,t} \beta_{D,j,t-1} \xi_{d,i,t-1} D_{exp,i,t-1} + \beta_{D,j,t} \xi_{d,i,t} \sum_{k=1}^{ND} \rho_{d,i,k} \beta_{D,j,t} \xi_{d,k,t} D_{exp,k,t}}}{r_{g,D,j,t}} + \sum_{j=1}^{N} \phi_{D,j,t} \frac{\gamma_{d,i,t,t-1} \beta_{D,j,t} \xi_{d,i,t} \beta_{U,j,t-1} \xi_{d,i,t-1} D_{exp,i,t-1} + \beta_{D,j,t} \xi_{d,i,t} \sum_{k=1}^{ND} \rho_{d,i,k} \beta_{D,j,t} \xi_{d,k,t} D_{exp,k,t}}}{r_{g,D,j,t+1}} + \sum_{j=1}^{N} \phi_{U,j,t+1} \frac{\gamma_{d,i,t,t+1} \beta_{U,j,t+1} \xi_{d,i,t+1} D_{exp,i,t+1} \beta_{D,j,t} \xi_{d,i,t} + \beta_{D,j,t} \xi_{d,i,t} \sum_{k=1}^{ND} \rho_{d,i,k} \beta_{D,j,t} \xi_{d,k,t} D_{exp,k,t}}}{r_{g,U,j,t+1}} + \sum_{j=1}^{N} \phi_{D,j,t+1} \frac{\gamma_{d,i,t,t+1} \beta_{D,j,t+1} \xi_{d,i,t+1} D_{exp,i,t+1} \beta_{U,i,t} \xi_{d,i,t} + \beta_{U,j,t} \xi_{d,i,t} \sum_{k=1}^{ND} \rho_{d,i,k} \beta_{U,j,t} \xi_{d,k,t} D_{exp,k,t}}}{r_{g,D,j,t+1}}}$$
(54)

 $U\_LMP\_PF$ ,  $U\_LMP\_G$ , and  $U\_LMP\_FRP$  are the components representing the uncertainty prices associated with the transmission power flow violation, generation limits violations, and generation ramping capability violations.  $U\_LMP\_FRP$  is the price that the uncertain demand should pay for the FRPs in the system. Note that when the demand has no uncertainty ( $\xi_{d,j,t}=0$ ), it will not pay these uncertainty prices. Note that in the  $U\_LMP$  formulation the value of the forecast uncertainty (standard deviation) is expressed as a percentage value of the forecast mean value. If the value of the standard deviation is represented by a constant instead, which is not associated with the value of its forecast mean, the  $U\_LMP$  still can be formulated using a similar approach.  $\xi_{d,j,t}$  and  $\xi_{w,j,t}$  represent the percentage of the standard deviation of demand and wind power to their forecast mean values, respectively.

The U\_LMP for the uncertain wind power can be derived in a similar manner, as shown in Eq. (55). Thus, in the proposed model, the uncertain demand and wind power will pay the controllable resources for the flexibility services to mitigate their uncertainty.

$$\begin{split} U_{-}LMP_{Wind,i,t} &= -\frac{\partial L(x)}{\partial P_{exp,i,t}} = \lambda_{t} + \sum_{l=1}^{M} GSF_{l-i} \left( \mu_{l,U,t}^{min} - \mu_{l,U,t}^{min} + \mu_{l,D,t}^{min} - \mu_{l,D,t}^{max} \right) - \\ & \qquad \qquad \qquad U_{-}LMP_{-}PF_{Wind,i,t} - \\ & \qquad \qquad \qquad U_{-}LMP_{-}G_{Wind,i,t} - \\ & \qquad \qquad \qquad U_{-}LMP_{-}FRP_{Wind,i,t} \end{split} \tag{55}$$

## V. CASE STUDIES

In this section, we carry out numerical simulations and studies for the proposed AAP-DRCC-MIOPF. First, a modified PJM 5-bus system is studied to illustrate the concept. Then, the IEEE 39-bus and IEEE 118-bus systems are tested. All of the simulations are performed in GAMS [26], which is widely utilized to solve large-scale complex optimization problems.

## A. PJM 5-Bus System

The PJM 5-bus system is depicted in Fig. 3, and the system parameters can be found in [27]–[30]. In this study, the system peak demand is 1,500 MW, and the total demand is distributed among buses B, C, and D equally. Two WPPs are located at bus B and bus C. The demand curve and two WPPs' forecast mean power curves are from CAISO at 6 a.m. on 02/01/2018 [31], shown in Fig. 4. The time interval is 5-minutes long, i.e. 12 intervals in one-hour simulation.

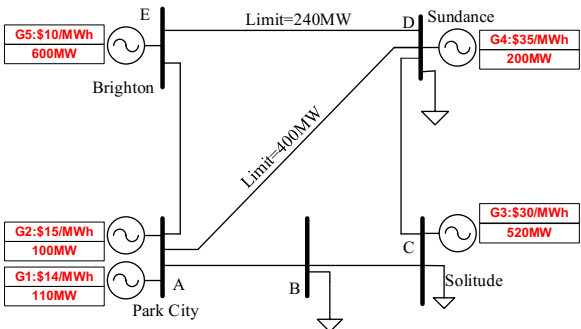


Fig. 3. PJM 5-bus system and generation parameters

1.000

0.980

0.960

0.940

0.920

0.900

1 2 3 4 5 6 7 8 9 10 11 12 200

Time interval (5 minutes)

Load WF1 WF2

Fig. 4. Demand and wind power curves

## B. Comparison between SAP and AAP

This subsection performs the comparison between the traditional SAP and the proposed AAP based DRCC-MIOPF models. The standard deviations of wind power and demand are assumed to be 10% and 3% of their forecasted expected values. Assuming that the forecasting errors of demand and wind power are following a Gaussian distribution, the confidence level of chance constraints are 95% ( $\epsilon = 0.05$ ). Then the value of  $K_{\epsilon}$  is 1.645 [22]. The distributional robustness of the forecasting errors will be investigated in subsection V.E.

The temporal correlation coefficients of demand and wind power are 0.6 and 0.9. The spatial correlation coefficients of demand and wind power are 0.5 and 0.6. The sensitivity of spatiotemporal correlation will be investigated in the subsection V.D. The generation schedules and their balancing factors are depicted in Fig. 5 and 6. Gen 5's actual generation output under different system imbalance conditions at various time intervals from the SAP and AAP models are shown in Fig. 7.

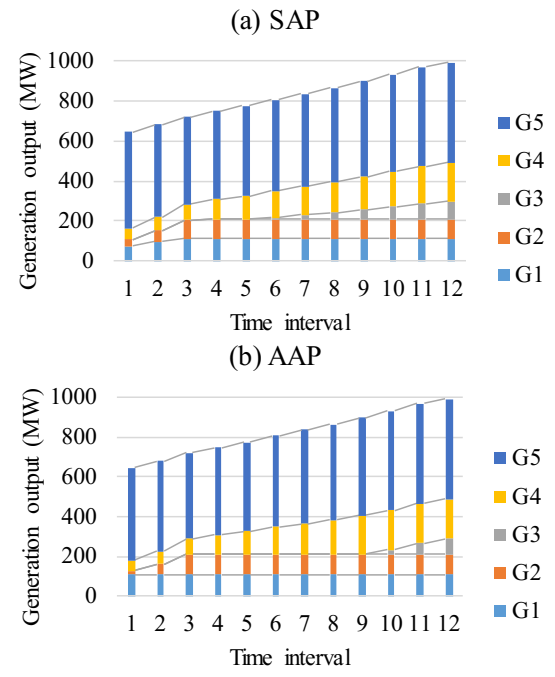


Fig. 5. Generation schedules with SAP and AAP CC-OPF

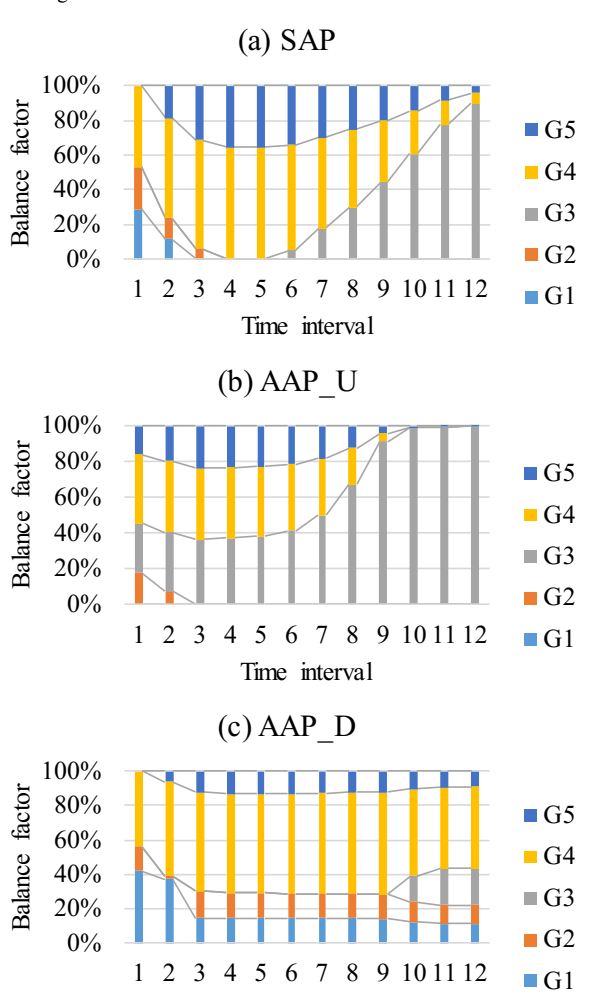


Fig. 6. Balance factors with SAP and AAP CC-OPF

Time interval

The system operating cost from SAP and AAP based DRCC-MIOPF models are \$155,567.9 and \$154,920.4. The

cost is thus reduced by 0.42% with the proposed AAP model. Therefore, by allowing the generation response to follow different uncertainty directions, the system operating costs can be reduced. Note that this cost saving will change with actual system conditions, especially the degree of the system ramping shortage. Additional studies about the generation costs from SAP and AAP models under different distribution assumptions will be investigated in subsection V.E.

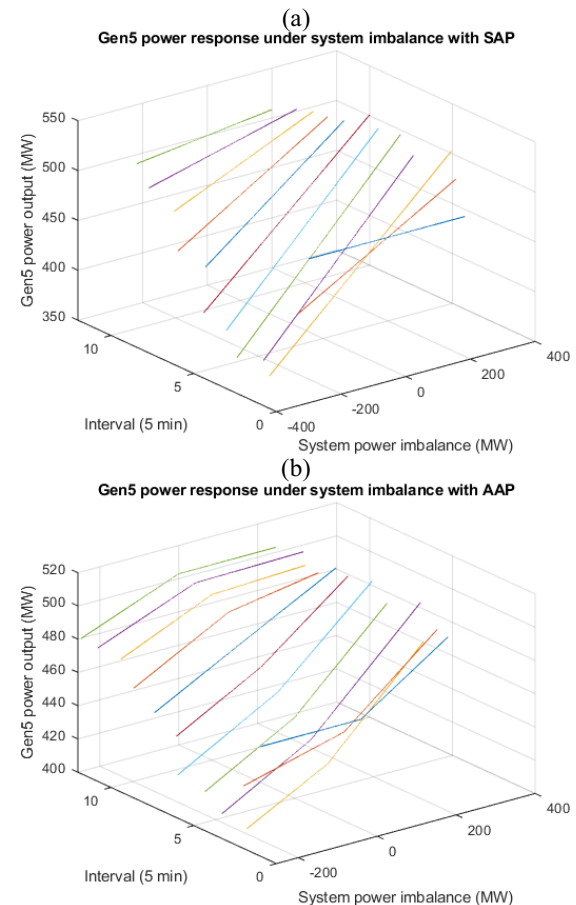


Fig. 7. Gen5 power response with SAP and AAP

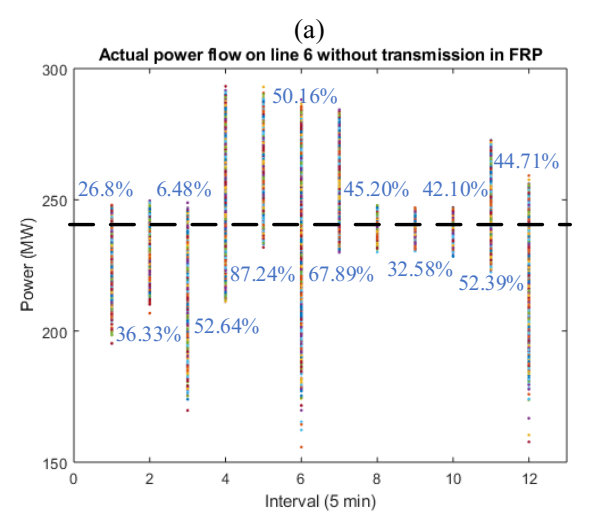
As shown in Fig. 5 and 6, the balancing factors change significantly, even though the difference in generation schedules is not very large. In the SAP model, G3 cannot provide the reserve from the 1<sup>st</sup> to the 6<sup>th</sup> intervals because its power output is at its lower limit during these intervals. In the AAP model, although G3's power output is still at the lower limit from the 1<sup>st</sup> and 9<sup>th</sup> intervals, it can provide the upward reserve as shown in Fig. 6(b). In addition, G1 provides the downward reserve with its power at the upper limit. Therefore, the proposed AAP-DRCC-MIOPF model provides more flexibility in the generation scheduling to mitigate the system uncertainty and reduce the operating cost.

Fig. 7 demonstrates Gen 5's power output under different system imbalance levels at different time intervals for the SAP and AAP models. It is obvious that in the SAP model the generation responses under the positive and the negative system imbalance are symmetrical (the slope does not change under the positive and the negative system imbalance) as shown in Fig. 7(a). While in Fig. 7(b), the slopes for the positive and negative response are different. Therefore, the generator can have

additional flexibility to mitigate the system imbalance due to the forecast errors based on the imbalance directions.

#### C. Deliverability of FRPs

This subsection studies the FRPs deliverability with the current FRPs model and the proposed model. To investigate the deliverability, the transmission power flow realization under the demand and wind power uncertainty is evaluated. The current FRPs model will be represented without the FRPs in the transmission power flow chance constrained limits. 10,000 samples of the demand and wind power at each interval are obtained using the Gaussian distribution to evaluate the actual power flow realization. Fig. 8 depicts the actual power flow on Line 6 with demand and wind power uncertainty realization at different time intervals.



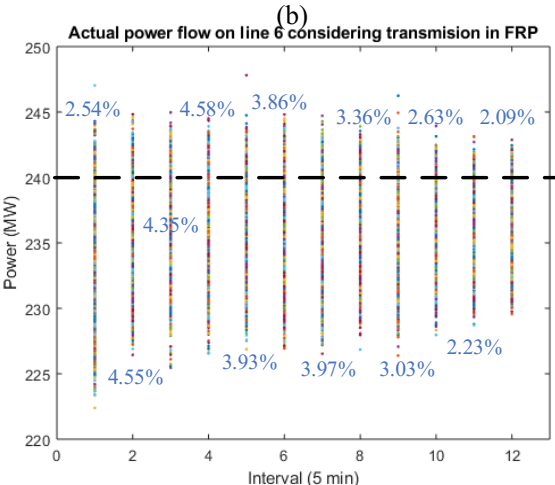


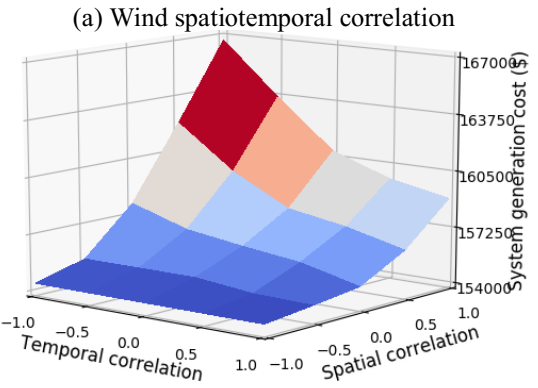
Fig. 8. Transmission power flow realization without/with considering FRPs in transmission constraints

The black dashed line shows the line capacity limit. The percentage numbers shown in Fig. 8 are the power flow limit violation probability at each interval. Fig. 8(a). presents the simulation results for 10,000 samples with the existing FRP model. It can be observed that the current FRPs model leads to significantly higher transmission overloading probabilities, compared with the proposed model. It shows that the chance of transmission overloading is as high as 87.24% and 11 out of 12 intervals have overloading in more than 30% of samples. In

contrast, Fig. 8 (b) shows no more than 4.58% of 10,000 samples have transmission overloading for all intervals, when the risk level is set to 5%. Therefore, the delivery of FRPs in the proposed model can be guaranteed within the predetermined risk level.

## D. Impacts of Spatiotemporal Correlation

The proposed model considers the spatiotemporal correlation of demand and wind power uncertainties. This subsection investigates the impacts of spatiotemporal correlation. The spatiotemporal correlations of demand and wind power uncertainties are simulated separately. The spatiotemporal correlation varies from -1 to 1 with 0.5 as the step change. The system operating costs under different spatiotemporal correlations are shown in Fig. 9.



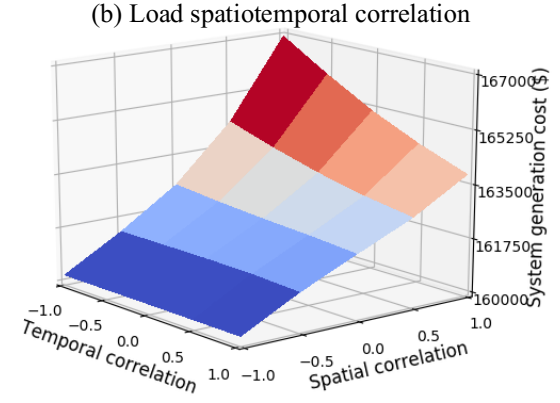


Fig. 9. System cost under various wind and demand spatiotemporal correlations

Fig. 9 illustrates that the system operating cost increases with the increment of spatial correlation of wind power uncertainties as well as that of demand uncertainties. In contrast, it reduces with the temporal correlation of wind power and demand. It can also be observed that the impact of the spatial correlation is higher than that of the temporal correlation for both the wind power and demand. For instance, when the temporal correlation coefficient of WPPs is 0, the costs increase 4.1% when the spatial correlation coefficient of wind increases from -1 to 1. When the spatial correlation coefficient of WPPs is 0, the cost decreases 1.77% when the temporal correlation coefficient of wind increases from -1 to 1.

From the FRPs formulation, the ramping requirement decreases with the temporal correlation monotonically. Therefore, the system operating cost reduces with temporal correlation. The variation of demands and WPPs power output

at each interval increase with the spatial correlation shown in Section II. Therefore, the cost increases with the spatial correlation. The temporal correlation affects the ramping constraints. The spatial correlation impacts all the constraints; thus, it has a higher impact on the system operating cost.

#### E. Distributional Robustness

This subsection analyzes the influence of the distributional robustness. The system generation costs and the FRPs costs of demands and WPPs are listed in Table I. The Bus C LMPs for the traditional generators, demand, and WPPs are depicted in Fig. 10. The generation costs of the SAP and AAP models under different distribution assumptions are listed in Table II.

Table I demonstrates that the system generation costs, and the FRPs costs of demands and WPPs increase with the chance constraints robustness to the forecast errors. With a higher robustness level, the system procures a higher reserve capacity to mitigate the uncertainty, therefore the operating cost and the FRPs costs increase with the robustness level.

Table I. 5-bus System Results Under Different Distributions

	Gaussian	Sym. Dist. R.	Dist. R
Gen Cost (\$)	154,920.4	159,728.1	165,458.3
Demand FRPs cost (\$)	7.726	1,674.8	4,416.7
Wind FRPs cost (\$))	29.266	5,274.7	12,626.4

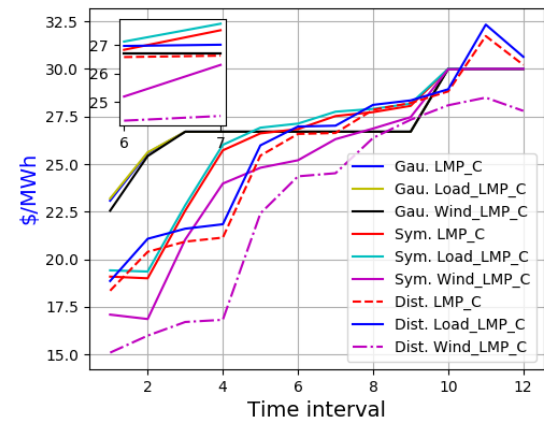


Fig. 10. Bus C LMPs under different distribution assumptions

Fig. 10 demonstrates the LMPs on Bus C for traditional generator, the uncertain demand and WPP. Regardless of the distribution assumptions, the demand LMP is the highest, the second highest is the traditional generation LMP, and the wind LMP is the lowest. Uncertain demands and WPPs pay a price for uncertainties because the system needs to procure additional resources to mitigate their uncertainties.

Table II. Generation Costs Results Under Different Distributions from SAP

and AAP			
	Gaussian	Sym. Dist. R.	Dist. R
SAP	155,567.9	161,367.8	167,010.9
AAP	154,920.4	159,728.1	165,458.3

Table II shows that the proposed AAP leads to a lower operation cost compared to the SAP model no matter what distribution assumption is used for the forecasting errors. In addition, with the increase of the robustness level, the cost saving increases. For instance, the cost reduces 0.42% from SAP to AAP in the Gaussian case. In the distributionally robust case, the cost reduces 0.94% from \$167,010.9 to \$165,458.3. This is because the system flexibility requirements increase with the distributional robustness. The proposed AAP model

gives additional flexibility to the generators compared to the SAP model to mitigate the uncertainty, which leads to lower costs. This implies that in a more flexibility constrained system the proposed AAP model will lead to a higher cost saving.

## F. IEEE 39-Bus System

The IEEE 39-bus system integrated with 3 WPPs is shown in Fig. 11. This system has ten generators with total capacity of 7,367 MW and a total demand of 6,254 MW. The detailed system parameters are in [32]. Three wind farms are integrated at buses 11, 24 and 26. The generation parameters are in [33]. Four thermal limits are applied to the following transmission lines: 800 MW for lines 1–39, 500 MW for lines 2–3, 500 MW for lines 3–18, and 600 MW for lines 16–17.

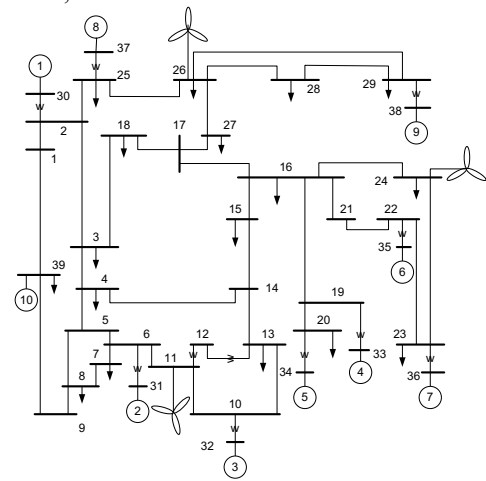


Fig. 11. IEEE 39-bus system with three WPPs

The demand curve is the same as in Fig. 4. The wind power curves are the same as in Fig. 4, with WPP1 at Bus 26 and WPP 2 at Bus 11. WPP3 at Bus 24 has the same output as WPP1. The confidence level of chance constraints is 95% [23]. The standard deviations of wind power and demand are assumed to be 3% and 1% of their forecasted expected values, respectively. The temporal correlation coefficients of demand and wind power are 0.4 and 0.3. The spatial correlation coefficient of wind power is 0.5. The spatial correlation of demand is ignored in this study.

Table II. IEEE 39-bus System Results Under Different Distributions

	Gaussian	Sym. Dist. R.	Dist. R
Gen Cost (\$)	1,057,289	1,060,661	1,063,726
Demand FRPs cost (\$)	0.669	2.583	18.512
Wind FRPs cost (\$))	200.229	624.873	2072.599

The system generation cost, FRPs costs of demand and wind power are listed in Table II. The LMPs on Bus 24 for the traditional generator, demand, and wind power are shown in Fig. 12. Similar to the study in the previous subsection, it is obvious that the system generation cost, the FRPs costs of demand and wind power increase with the distributional robustness. From Fig. 12, it shows that the LMPs for the traditional generator, demand, and wind power change with the distributional robustness level. In all distribution cases, the demand has the highest LMP, and wind power has the lowest. In this figure, it also shows that the price volatility increases with the robustness level for the forecast errors. Because the system is more constrained and tighter of flexibility under a

high robustness case, then the shadow price for the flexibility increases.

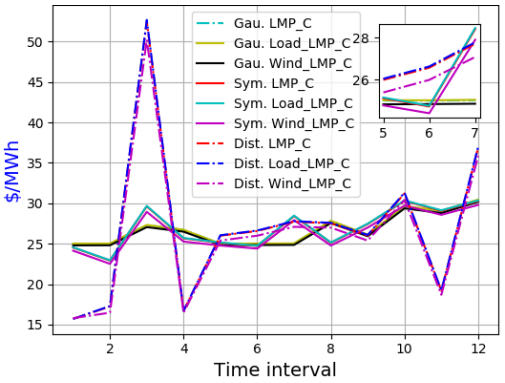


Fig. 12. Bus 24 LMPs under different distribution assumptions

#### G. IEEE 118-Bus System

To test the proposed model in a large system, the IEEE 118-bus system is used. The system data can be found in [29]. Four WPPs are connected at Bus 46, Bus 80, Bus 87, and Bus 111. The demand curve is the same as in Fig. 4. The wind power curves are the same as in Fig. 4, with WPP1 at Bus 46 and WPP 2 at Bus 80. WPP3 at Bus 87 has the same output as WPP1, and WPP4 at Bus 111 has the same output as WPP2. The standard deviations of wind power and demand are assumed to be 4% and 2% of their forecasted expected values, respectively. The system simulation results under different distribution assumptions for the forecasting errors are listed in Table III.

Table III. IEEE 118-bus System Results Under Different Distributions

	Gaussian	Sym. Dist. R.	Dist. R
Gen Cost (\$)	113675.1	114961.8	116331.5
Demand FRPs cost (\$)	12.8	28.6	30.1
Wind FRPs cost (\$))	103.4	517.9	1490.5

Table III demonstrated that the system generation cost increases monotonically with the conservativeness of the forecasting errors. High conservativeness leads to high reserve capacity procurement. For the FRPs cost of demand and wind power, they are also increasing with the conservativeness of the forecasting errors.

#### H. Computational Performance

All the case studies are performed in GAMS with MOSEK as the quadratically constrained programming (QCP) solver [26], [34]. A Dell laptop with computer processing unit Intel Core i5 is used for all the case studies. The average computational times for different systems are listed in Table III. The computational time of all the cases of the 5-bus system are less than 1 second. For the 39-bus system, the optimal solutions can be obtained within 2 seconds for all cases. The solutions of 118-bus system can be obtained in around 5 seconds as shown in Table IV. To accelerate the proposed model for large systems, there are two approaches. First, reduce the number of intervals in the model. There are 12 look-ahead time intervals

in the proposed RTED model. While in the actual RTED model of ISOs, the number of the look-ahead intervals is smaller and can be adjusted based on the system conditions. We investigated that the computation time was reduced to less than 1 second when the number of intervals was reduced from 12 to 6 in the 39-bus system. Because the forecasting for the later 6 intervals is not as accurate as the previous 6 intervals, to schedule more reserve for the longer time horizon can be very costly. Second, with the 12 intervals unchanged, but only considering the uncertainty in the first 6 intervals can lead to a similar computational time reduction. In addition, the iterative solution procedure introduced in [13] and the decentralized optimization in [30] can be used to accelerate the proposed model. This is left to the future work.

Table IV. Average computational time of different cases			
	PJM 5-bus	IEEE 39-bus	IEEE 118-bus
Comp. Time (s)	0.4	1.3	5.1

#### VI. CONCLUSIONS

This paper proposes a deliverable flexible ramping products model considering the spatiotemporal correlation of uncertain wind power and demand. Because all of the system security constraints are modeled, the proposed FRPs are deliverable in the real time operation. An asymmetrical affine policy (AAP) is proposed for the generators to mitigate the demand and wind power forecasting errors based on the imbalance directions. It shows that the proposed AAP-DRCC-MIOPF model leverages the generation flexibility to mitigate the uncertainty of different directions and reduces the system cost. The uncertainty contained LMP (U\_LMP) is derived including the price signals for the FRPs. The uncertain demand and wind power can pay this price based on their locations, and uncertainty level to the system operators to procure the FRPs.

How to procure adequate flexible resources in the system operation and price the system uncertainty efficiently are two significant issues under a high penetration level of renewable integration such as wind power. The model proposed in this paper can obtain the deliverable FRPs in the forward market to mitigate the uncertainty of both demand and wind power. The spatiotemporal correlation is endogenously considered, which can help to evaluate the system ramping requirement accurately. The derived U\_LMP can be used to price the uncertainties of wind power and demand and compensate the flexible resources in the system.

#### **APPENDIX**

The Lagrange function of the model in (46) is expanded in Eq. (A1). The partial derivative of the Lagrange function to the demand at bus i is shown in Eq. (A2). Note that here the uncertainty component of demands (its standard deviation) is expressed as a percentage value of its forecast mean value.

$$L(x) = \sum_{t=1}^{T} \left\{ \sum_{i=1}^{N} c_{i,t} G_{exp,i,t} - \lambda_{t} \left( \sum_{i=1}^{N} (G_{exp,i,t} + P_{exp,i,t}) - \sum_{i=1}^{N} D_{exp,i,t} \right) - \sum_{l=1}^{M} \mu_{l,U,t}^{max} \left[ - \sum_{i=1}^{N} GSF_{l,i} \left( G_{exp,i,t} + P_{exp,i,t} - D_{exp,i,t} \right) - \sum_{l=1}^{N} \mu_{l,U,t}^{max} \left[ - \sum_{i=1}^{N} GSF_{l,i} \left( G_{exp,i,t} + P_{exp,i,t} - D_{exp,i,t} \right) - K_{\epsilon} \eta_{PF,U,l,t} + LU_{l} \right] - \sum_{l=1}^{M} \mu_{l,D,t}^{max} \left[ - \sum_{i=1}^{N} GSF_{l,i} \left( G_{exp,i,t} + P_{exp,i,t} - D_{exp,i,t} \right) - K_{\epsilon} \eta_{PF,D,l,t} + LU_{l} \right] - \sum_{l=1}^{M} \mu_{l,D,t}^{min} \left[ \sum_{i=1}^{N} GSF_{l,i} \left( G_{exp,i,t} + P_{exp,i,t} - D_{exp,i,t} \right) - K_{\epsilon} \eta_{PF,D,l,t} + LU_{l} \right] - \sum_{l=1}^{M} \mu_{l,D,t}^{min} \left[ \sum_{i=1}^{N} GSF_{l,i} \left( G_{exp,i,t} + P_{exp,i,t} - D_{exp,i,t} \right) - K_{\epsilon} \eta_{PF,D,l,t} + LU_{l} \right] - \sum_{l=1}^{M} \mu_{l,D,t}^{min} \left[ \sum_{i=1}^{N} GSF_{l,i} \left( G_{exp,i,t} + P_{exp,i,t} - D_{exp,i,t} \right) - K_{\epsilon} \eta_{PF,D,l,t} + LU_{l} \right] - \sum_{l=1}^{M} \mu_{l,D,t}^{min} \left[ \sum_{i=1}^{N} GSF_{l,i} \left( G_{exp,i,t} + P_{exp,i,t} - D_{exp,i,t} \right) - K_{\epsilon} \eta_{PF,D,l,t} + LU_{l} \right] - \sum_{l=1}^{M} \mu_{l,D,t}^{min} \left[ \sum_{i=1}^{N} GSF_{l,i} \left( G_{exp,i,t} + P_{exp,i,t} - D_{exp,i,t} \right) - K_{\epsilon} \eta_{PF,D,l,t} + LU_{l} \right] - \sum_{l=1}^{M} \mu_{l,D,t}^{min} \left[ \sum_{i=1}^{N} GSF_{l,i} \left( G_{exp,i,t} + P_{exp,i,t} - D_{exp,i,t} \right) - K_{\epsilon} \eta_{PF,D,l,t} + LU_{l} \right] - \sum_{l=1}^{M} \mu_{l,D,t}^{min} \left[ \sum_{i=1}^{N} GSF_{l,i} \left( G_{exp,i,t} + P_{exp,i,t} - D_{exp,i,t} \right) - K_{\epsilon} \eta_{PF,D,l,t} + LU_{l} \right] \right] - \sum_{l=1}^{M} \mu_{l,D,t}^{min} \left[ \sum_{i=1}^{N} GSF_{l,i} \left( G_{exp,i,t} + P_{exp,i,t} - D_{exp,i,t} \right) \right] - \sum_{l=1}^{M} \mu_{l,D,t}^{min} \left[ \sum_{i=1}^{N} GSF_{l,i} \left( G_{exp,i,t} + D_{exp,i,t} \right) \right] - \sum_{l=1}^{M} \mu_{l,D,t}^{min} \left[ \sum_{i=1}^{N} GSF_{l,i} \left( G_{exp,i,t} + D_{exp,i,t} \right) \right] - \sum_{l=1}^{M} \mu_{l,D,t}^{min} \left[ \sum_{i=1}^{N} GSF_{l,i} \left( G_{exp,i,t} + D_{exp,i,t} \right) \right] \right] \right]$$

$$\begin{split} &P_{exp,l,t} - D_{exp,l,t} - K_{e}\eta_{pF,D,l,t} + LU_{l} - \sum_{l=1}^{N} \omega_{l,t}^{imax} \left( -G_{l} - K_{e}\eta_{g,D,l,t} + G_{l}^{imax} \right) - \sum_{l=1}^{N} \omega_{l,t}^{iim} \left( G_{l} - K_{e}\eta_{g,D,l,t} - G_{l}^{imax} \right) - \sum_{l=1}^{N} \tau_{l,t}^{iim} \left( R_{l}^{i} \cdot \Delta t - G_{exp,l,t} - G_{exp,l,t-1} - K_{e}r_{g,U,l,t} - \sum_{l=1}^{N} \tau_{l,t}^{iin} \left( R_{l}^{i} \cdot \Delta t + G_{exp,l,t-1} - G_{exp,l,t-1} - K_{e}r_{g,U,l,t} - \sum_{l=1}^{N} \tau_{l,t}^{iin} \left( R_{l}^{i} \cdot \Delta t + G_{exp,l,t-1} - G_{exp,l,t-1} - K_{e}r_{g,U,l,t} - \sum_{l=1}^{N} \tau_{l,t}^{iin} \left( R_{l}^{i} \cdot \Delta t + G_{exp,l,t-1} - G_{exp,l,t-1} - K_{e}r_{g,D,l,t} \right) \\ & \left\| \left[ \sum_{u,t}^{1/2} \left\| b_{u,l,t} \left( \beta_{D,t} \right) \right\|_{2} \right] - \sum_{l=1}^{N} \left\| b_{g,U,l,t} \left( \eta_{g,U,l,t} - \left\| \sum_{u,t}^{2} v_{l}^{1/2} \right\| b_{u,l,t} \left( \beta_{U,t} \right) \right\|_{2} \right) + \Phi_{D,l,t} \left( \eta_{g,D,l,t} - \left\| \sum_{u,t}^{2} v_{l}^{1/2} \right\| b_{u,l,t} \left( \beta_{D,t} \right) \right\|_{2} \right) + \Phi_{D,l,t} \left( \eta_{g,D,l,t} - \left\| \sum_{u,t}^{2} v_{l}^{1/2} \right\| b_{u,l,t} \left( \beta_{D,t} \right) \right\|_{2} \right) + \Phi_{D,l,t} \left( r_{g,U,l,t} - \left\| \sum_{u,t}^{2} v_{l}^{1/2} \right\| b_{u,l,t} \left( \beta_{D,t} \right) \right\|_{2} \right) + \Phi_{D,l,t} \left( r_{g,U,l,t} - \left\| \sum_{u,t}^{2} v_{l}^{1/2} \right\| b_{u,l,t} \left( \beta_{D,t} \right) \right\|_{2} \right) + \Phi_{D,l,t} \left( r_{g,U,l,t} - \left\| \sum_{u,t}^{2} v_{l}^{1/2} \right\| b_{u,l,t} \left( \beta_{D,t} \right) \right\|_{2} \right) + \Phi_{D,l,t} \left( r_{g,U,l,t} - \left\| \sum_{u,t}^{2} v_{l}^{1/2} \right\| b_{u,l,t} \left( \beta_{D,t} \right) \right\|_{2} \right) + \Phi_{D,l,t} \left( r_{g,U,l,t} - \left\| \sum_{u,t}^{2} v_{l}^{1/2} \right\| b_{u,l,t} \left( \beta_{D,t} \right) \right\|_{2} \right) + \Phi_{D,l,t} \left( r_{g,U,l,t} - \left\| \sum_{u,t}^{2} v_{l}^{1/2} \right\| b_{u,l,t} \left( \beta_{D,t} \right) \right\|_{2} \right) + \Phi_{D,l,t} \left( r_{g,U,l,t} - \left\| \sum_{u,t}^{2} v_{l}^{1/2} \right\| b_{u,l,t} \left( \beta_{D,t} \right) \right\|_{2} \right) + \Phi_{D,l,t} \left( r_{g,U,l,t} - \left\| \sum_{u,t}^{2} v_{l}^{1/2} \right\| b_{u,l,t} \left( \beta_{D,t} \right) \right\|_{2} \right) + \Phi_{D,l,t} \left( r_{g,U,l,t} - \left\| \sum_{u,t}^{2} v_{l}^{1/2} \right\| b_{u,l,t} \left( \beta_{D,t} \right) \right\|_{2} \right) + \Phi_{D,l,t} \left( r_{g,U,l,t} - \left\| \sum_{u,t}^{2} v_{l}^{1/2} \right\| b_{u,l,t} \left( \beta_{D,t} \right) \right\|_{2} \right) + \Phi_{D,l,t} \left( r_{g,U,l,t} - \left\| \sum_{u,t}^{2} v_{l}^{1/2} \right\| b_{u,l,t} \left( \beta_{D,t} \right) \right\|_{2} \right) + \Phi_{D,l,t} \left( r_{g,U,l,t} - \left\| \sum_{u,t}^{2} v_{l}^{1/2} \right\| b_{u$$

## ACKNOWLEDGEMENT

The views expressed in the article do not necessarily represent the views of the DOE or the U.S. Government. The U.S. Government retains and the publisher, by accepting the article for publication, acknowledges that the U.S. Government retains a nonexclusive, paid-up, irrevocable, worldwide license to publish or reproduce the published form of this work, or allow others to do so, for U.S. Government purposes.

## REFERENCES

- [1] California ISO, "Flexible Ramping Product." 2016.
- [2] N. Navid and G. Rosenwald, "Ramp Capability Product Design for MISO Markets," Mid-Continent System Operator, 2013.
- [3] Q. Chen et al., "A Nash-Cournot approach to assessing flexible ramping products," Applied Energy, vol. 206, no. December 2016, pp. 42–50, 2017
- [4] M. Cui, D. Ke, Y. Sun, D. Gan, J. Zhang, and B.-M. Hodge, "Wind Power Ramp Event Forecasting Using a Stochastic Scenario Generation Method," *IEEE Transactions on Sustainable Energy*, vol. 6, no. 2, pp. 422–433, 2015.
- [5] R. Chen, J. Wang, A. Botterud, and H. Sun, "Wind Power Providing Flexible Ramp Product," *IEEE Transaction on Power Systems*, vol. 32, no. 3, pp. 2049–2061, 2017.
- [6] Y. Chen, P. Gribik, and J. Gardner, "Incorporating Post Zonal Reserve Handle Forecast Uncertainty: A Chance Constrained Optimal Power Flow,"

- Deployment Transmission Constraints Into Energy and Ancillary Service Co-Optimization," *IEEE Transactions on Power Systems*, vol. 29, no. 2, pp. 537–549, 2014.
- [7] H. Ye and Z. Li, "Deliverable Robust Ramping Products in Real-Time Markets," *IEEE Transactions on Power Systems*, vol. 33, no. 1, pp. 5– 18, 2018.
- [8] H. Ye, Y. Ge, M. Shahidehpour, and Z. Li, "Uncertainty Marginal Price, Transmission Reserve, and Day-Ahead Market Clearing with Robust Unit Commitment," *IEEE Transactions on Power Systems*, vol. 32, no. 3, pp. 1782–1795, 2017.
- [9] M. Cui, J. Zhang, C. Feng, A. R. Florita, Y. Sun, and B. M. Hodge, "Characterizing and analyzing ramping events in wind power, solar power, load, and netload," *Renewable Energy*, vol. 111, pp. 227–244, 2017.
- [10] K. Porter, K. Starr, and A. Mills, "Variable Generation and Electricity Markets," 2015.
- [11] K. Sundar et al., "Unit commitment with N-1 Security and wind uncertainty," *IEEE Transactions on control of network systems*, vol. PP, no. 8, pp. 1–12, 2019.
- [12] K. Sundar et al., "Unit commitment with N-1 Security and wind uncertainty," 19th Power Systems Computation Conference, PSCC 2016, pp. 1–7, 2016.
- [13] L. Roald and G. Andersson, "Chance-Constrained AC Optimal Power Flow: Reformulations and Efficient Algorithms," *IEEE Transactions on Power Systems*, vol. 33, no. 3, pp. 2906–2918, 2018.
- [14] M. Lubin, Y. Dvorkin, and L. Roald, "Chance constraints for improving the security of ac optimal power flow," *IEEE Transactions on Power Systems*, vol. 34, no. 3, pp. 1908–1917, 2019.
- [15] L. Roald, S. Misra, T. Krause, and G. Andersson, "Corrective Control to IEEE Transactions on Power Systems, vol. 32, no. 2, pp. 1626–1637,

- 2017.
- [16] Y. Zhang, S. Shen, and J. L. Mathieu, "Distributionally Robust Chance-Constrained Optimal Power Flow with Uncertain Renewables and Uncertain Reserves Provided by Loads," IEEE Transactions on Power Systems, vol. 32, no. 2, pp. 1378-1388, 2017.
- [17] C. Duan, W. Fang, L. Jiang, L. Yao, and J. Liu, "Distributionally Robust Chance-Constrained Approximate AC-OPF with Wasserstein Metric," IEEE Transactions on Power Systems, vol. 8950, no. c, pp. 1–12, 2018.
- [18] B. Li, R. Jiang, and J. L. Mathieu, "Distributionally Robust Chance Constrained Optimal Power Flow Assuming Log-Concave Distributions," IEEE Transactions on control of network systems, no. September, 2018.
- [19] "Normal distribution." [Online]. Available: https://en.wikipedia.org/wiki/Normal distribution.
- [20] M. Vrakopoulou, B. Li, and J. L. Mathieu, "Chance Constrained Reserve Scheduling Using Uncertain Controllable Loads Part I: Formulation and Scenario-based Analysis," IEEE Transactions on Smart Grid, vol. PP, no. 99, pp. 1-9, 2018.
- [21] L. Roald, S. Misra, M. Chertkov, and G. Andersson, "Optimal Power Flow with Weighted chance constraints and general policies for generation control," Proceedings of the IEEE Conference on Decision and Control, vol. 54rd IEEE, no. Cdc, pp. 6927-6933, 2015.
- [22] G. C. Calafiore and L. El Ghaoui, "On distributionally robust chanceconstrained linear programs," Journal of Optimization Theory and Applications, vol. 130, no. 1, pp. 1-22, 2006.
- [23] X. Fang, H. Cui, H. Yuan, J. Tan, and T. Jiang, "Distributionally-robust chance constrained and interval optimization for integrated electricity and natural gas systems optimal power flow with wind uncertainties,' Applied Energy, vol. 252, no. October, pp. 1–13, 2019.
- [24] T. Zheng and E. Litvinov, "Contingency-based zonal reserve modeling and pricing in a co-optimized energy and reserve market," IEEE Transactions on Power Systems, vol. 23, no. 2, pp. 277-286, 2008.

- [25] Y. Chen, R. Leonard, M. Keyser, and J. Gardner, "Development of performance-based two-part regulating reserve compensation on miso energy and ancillary service market," IEEE Transactions on Power Systems, vol. 30, no. 1, pp. 142-155, 2015.
- "GAMS," 2018. [Online]. Available: http://www.gams.com/.
- X. Fang, F. Li, Y. Wei, and H. Cui, "Strategic scheduling of energy [27] storage for load serving entities in locational marginal pricing market," IET Gener., Transm. & Distrib., vol. 10, no. 5, pp. 1258–1267, 2016.
- X. Fang, B.-M. Hodge, E. Du, C. Kang, and F. Li, "Introducing Uncertainty Components in Locational Marginal Prices for Pricing Wind Power and Load Uncertainties," IEEE Transactions on Power Systems, vol. 34, no. 3, pp. 2013–2024, May 2019.
- [29] X. Fang, B.-M. Hodge, E. Du, N. Zhang, and F. Li, "Modelling wind power spatial-temporal correlation in multi-interval optimal power flow: A sparse correlation matrix approach," Applied Energy, vol. 230, pp. 531-539, Nov. 2018.
- X. Fang, B. M. Hodge, H. Jiang, and Y. Zhang, "Decentralized wind uncertainty management: Alternating direction method of multipliers based distributionally-robust chance constrained optimal power flow," Applied Energy, vol. 239, pp. 938–947, 2019. "California ISO|OASIS," 2018. [Online]. Available:
- http://oasis.caiso.com/mrioasis/logon.do.
- [32] X. Fang, F. Li, and N. Gao, "Probabilistic Available Transfer Capability Evaluation for Power Systems with High-Penetration Wind Power," in 13th International Conference on Probabilistic Methods Applied to Power Systems (PMAPS), 2014, pp. 1-6.
- [33] X. Fang, F. Li, Q. Hu, and Y. Wei, "Strategic CBDR Bidding Considering FTR and Wind Power," IET Gener., Transm. & Distrib., vol. 10, no. 10, pp. 2464–2474, 2016.
- "MOSEK," 2018. [Online]. Available: http://www.gamsworld.org/cone/solvers.htm#MOSEK.